# Amplification of light absorption of black carbon associated with air pollution

Yuxuan Zhang[1,2], Qiang Zhang[1], Yafang Cheng[3,2], Hang Su[3,2], Haiyan Li[4], Meng Li[1,2], Xin Zhang[1], Aijun Ding[5], and Kebin He[4]

[1]Ministry of Education Key Laboratory for Earth System Modeling, Department of Earth System Science, Tsinghua University, Beijing 100084, China

[2]Multiphase Chemistry Department, Max Planck Institute for Chemistry, Mainz 55020, Germany

[3]Institute for Environmental and Climate Research, Jinan University, Guangzhou 510630, China

[4]State Key Joint Laboratory of Environment Simulation and Pollution Control, School of Environment, Tsinghua University, Beijing 100084, China

[5]Institute for Climate and Global Change Research, School of Atmospheric Sciences, Nanjing University, Nanjing, China

*Correspondence to*: Qiang Zhang (qiangzhang@tsinghua.edu.cn)

**Abstract.** The impacts of black carbon (BC) aerosols on air quality, boundary layer dynamic and climate depend not only on the BC mass concentration but also on the light absorption capability of BC. It is well known that the light absorption capability of BC depends on the amount of coating materials (namely other species on BC by condensation and coagulation). However, the difference of light absorption capability of ambient BC-containing particles under different air pollution conditions (e.g., the air clean and polluted conditions) remains unclear due to the complex aging process of BC in the atmosphere. In this work, we investigated the evolution of light absorption capability for BC-containing particles with changing pollution levels in urban Beijing, China. During the campaign period (17 to 30 November 2014), with the growth of $PM_1$ concentration from ~10 μg m$^{-3}$ to ~230 μg m$^{-3}$, we found that the mass-weighted averages of the aging degree and theoretical light absorption capability of BC-containing particles increased by ~33% and ~18%, respectively, indicating stronger light absorption capability of BC-containing particles under more polluted conditions due to more coating materials on the BC surface. By using effective emission intensity (EEI) model, we further found that aging during the regional transport plays an important role in the difference among the light absorption capability of BC-containing particles under different air pollution levels. During the pollution episode, ~63% of the BC over Beijing originated from regional sources outside of Beijing. These regionally sourced BC-containing particles were characterized by more coating materials on BC surface due to more coating precursors within more polluted air, which contributed ~75% of the increase in theoretical light absorption capability of BC observed in Beijing during the polluted period ($PM_1$ of ~230 μg m$^{-3}$) comparing to that in the clean period ($PM_1$ of ~10 μg m$^{-3}$). Due to the increase

1  of theoretical light absorption capability of BC associated with air pollution, the direct radiative forcing of BC was estimated

2  to be increased by ~18% based on a simple radiation transfer model. Our work identified an amplification of theoretical light

3  absorption and direct radiative forcing under more air polluted environment due to more coating pollutants on BC. The air

4  pollution control measures may, on the other hand, break the amplification effect by reducing emissions of both BC and the

5  coating materials and achieve co-benefits of both air quality and climate.

6  **1 Introduction**

7  Black carbon (BC) is an important aerosol component that absorbs visible sunlight and contributes to heating of the atmosphere

8  (Bond and Bergstrom, 2006; Gustafsson and Ramanathan, 2016; Menon et al., 2002). Atmospheric BC can impact climate

9  through radiative effects, which are strongly associated with the optical properties of BC, especially the light absorption (Cheng

10  et al., 2006; Jacobson, 2000; Lesins et al., 2002; Ramanathan and Carmichael, 2008). Estimating the climate effects of BC is

11  one of the major challenges in climate change research, partly due to large uncertainties in the light absorption capability of

12  BC-containing particles under ambient conditions (Cappa et al. 2012; Liu et al. 2015; Liu et al. 2017; Gustafsson and

13  Ramanathan, 2016). The light absorption capability of atmospheric BC is complex and poorly quantified, and it changes with

14  the morphology, density and mixing state of the BC-containing particles (Knox et al., 2009; Peng et al. 2016; Schnaiter et al.

15  2005; Zhang et al., 2008). Previous theoretical (Jacobson, 2001; Moffet et al., 2009; Zhang et al., 2016) and observation studies

16  (Cappa et al., 2012; Peng et al., 2016; Knox et al., 2009) studies showed a broad range of absorption enhancements (1.05-3.05)

17  of BC-containing particles during the atmospheric aging process. To date, conflicts remain between model- and observation-

18  based studies of the light absorption capability of atmospheric BC-containing particles (Cappa et al., 2012; Jacobson, 2001;

19  Liu et al. 2015; Liu et al. 2017).

20  The light absorption capability of BC-containing particles depends strongly on the particle mixing state (Liu et al. 2015;

21  Liu et al. 2017), i.e., the degree of internal mixing between BC and other particle species (i.e., non-BC components) by the

22  atmospheric aging process (i.e., condensation, coagulation and heterogeneous oxidation). The non-BC species (i.e., coating

23  materials) on the surface of BC cores can enhance BC light absorption via the lensing effect (namely, the coating materials act

24  as a lens to focus more photons on BC, Bond et al., 2006; Fuller et al., 1999; Jacobson, 2001; Lack and Cappa, 2010). In terms

25  of individual BC-containing particle, more coating materials result in its stronger light absorption capability. The coating

26  materials on the BC surface are controlled by secondary processes (e.g., photochemical production) (Metcalf et al., 2013).

27  The production of secondary aerosols in the atmosphere varies significantly with pollution levels (Cheng, 2008; Zheng et

28  al., 2016; Yang et al., 2015), indicating that BC-containing particles most likely exert different light absorption capability

29  values under different pollution levels. Compared with air clean conditions, polluted periods feature more secondary aerosols,

30  especially secondary inorganic species such as sulfate (Guo et al., 2014; Sun et al., 2014; Zheng et al., 2015). Whether the

31  changes of secondary aerosols with air pollution will affect the coating materials on the BC is complex, which not only depends

32  on the increase in BC amount versus secondary aerosols but also controlled by secondary material condensation on BC versus

non-BC containing particles.  Recent BC aging measurements in Beijing and Houston using an environmental chamber (flowing ambient air to feed with lab-generated fresh BC) have revealed that a clear distinction in the light absorption capability of BC-containing particles exists between urban cities in developed and developing countries (Peng et al., 2016), and this difference is likely due to the differences in air pollution levels.

To date, whether and how the aging degree and light absorption capability of BC-containing particles will change with air pollution development is still unclear.  Although the enhancement of BC light absorption due to coating materials on BC surface has already been intensively investigated (Moffet et al., 2009; Schnaiter et al., 2005; Shiraiwa et al., 2010; Zhang et al., 2016), there are few studies on the evolution of the light absorption capability of  BC-containing particles with changing air pollution levels. The variation in the light absorption capability of BC-containing particles associated with air pollution can lead to different effects of BC aerosols on air quality and climate under different pollution levels. To improve the evaluation of BC-related effects on air quality and climate, some models have considered BC internally mixed with other species (namely coating materials on BC surface), which can affect the light absorption capability of BC-containing particles. However, the difference of coating materials on BC under different air pollution conditions remains unclear.

In this work, we conducted an intensive field measurement campaign in urban Beijing, China, to investigate the difference of the theoretical light absorption capability of atmospheric BC-containing particles under different pollution levels. Firstly, we analyzed the evolution of theoretical light absorption capability of BC with increasing air pollution levels and estimated the relationship between the rates of changes in the theoretical light absorption capability of BC and in the $PM_1$ or BC mass concentrations. We then explored the cause of the evolution of theoretical light absorption capability of BC with increasing air pollution levels and evaluated the relative importance of regional transport. Finally, we discussed the impact of changes in BC light absorption capability with pollution levels on BC radiative forcing.

## 2 Methods

### 2.1 Sampling site and measurements

The *in-situ* measurements were conducted on the campus of Tsinghua University (Tsinghua site, 40º00'17" N, 116º19'34" E) from November 17-30, 2014. The Tsinghua site (Fig. S1) is located in urban Beijing, China. The megacity Beijing is adjacent to Hebei Province and the megacity Tianjin (Fig. S1), in which considerable industrial manufacturing has led to heavy emissions of air pollution, especially in southern Hebei.

Ambient aerosol particles were collected by a $PM_1$ cyclone and then passed through a diffusion silica gel dryer, and they were finally analyzed by an aethalometer (AE33, Magee Scientific Corp.), an Aerosol Chemical Speciation Monitor (ACSM, Aerodyne Research Inc.) and a single particle soot photometer (SP2, Droplet Measurement Technologies Inc.). The AE33 can measure the absorption coefficient ($\sigma_{ab}$) of sampled aerosols in seven spectral regions (370, 470, 520, 590, 660, 880 and 950 nm). At a wavelength of 880 nm, the absorption of aerosol particles is dominated by BC component because the light absorbed

by other aerosol components is significantly less (Drinovec et al., 2015; Sandradewi et al., 2008). In this study, the $\sigma_{ab}$ at 880 nm measured by the AE33 was used to characterize the theoretical light absorption of the BC-containing particles. More details on the AE33 measurement can be found in the work of Drinovec et al., 2015. Considering the filter-loading effect and multiple-scattering effect (Drinovec et al., 2015; Weingartner et al., 2003; Segura et al., 2014), the aethalometer data was corrected by compensation factors described in the supplementary information (Fig. S2 and the associated discussion). The ACSM and SP2 instruments measured the mass concentrations of non-refractory submicron-scale components (NR-PM1, i.e., sulfate, nitrate, ammonium, chloride and organics) and refractory BC (rBC), respectively, and the sum of these two measurements was used to estimate the $PM_1$ mass concentration. The ACSM instrument used in our study was described by Li et al. (2017).

The SP2 instrument measures a single BC-containing particle using a 1064 nm Nd:YAG intra-cavity laser beam. As the light-absorbing rBC passes through the laser beam and is heated to its vaporization temperature (~4000 K), it will emit incandescent light (i.e., visible thermal radiation), which is linearly proportional to the mass of the rBC (Metcalf et al., 2012; Moteki and Kondo, 2010; Schwarz et al., 2006; Sedlacek et al., 2012). In this study, the calibration curve of rBC mass vs. incandescence signal was obtained from the incandescence signal of size-resolved Aquadag particles (their effective density obtained from Gysel et al., 2011) using a DMA (differential mobility analyzers)-SP2 measurement system. Considering different sensitive of the SP2 to different rBC types (Gysel et al., 2011; Laborde et al., 2012), we corrected SP2 calibration curve by scaling the peak height of incandescence signal for Aquadag particles at each rBC mass based on the relationship between the sensitivity of SP2 to Aquadag and ambient rBC (Laborde et al., 2012). The particle-to-particle mass of ambient rBC can be determined by measuring its incandescence signal and comparing it to the calibration curve. The mass concentration of rBC is calculated from the particle-to-particle mass of rBC and the sampled flow (~0.12 lpm). Note that the SP2 detection efficiency (Fig. S3) have been considered in the calculation of rBC mass concentration. Furthermore, the scattering cross section of a BC-containing particle is obtained from its scattering signal using the leading edge only (LEO)-fit method (Gao et al. 2007). Zhang et al. (2016) has demonstrated the validity of the LEO-fit method for ambient BC-containing particles in China.

**2.2 SP2 data analysis**

**2.2.1 Aging degree of BC-containing particles**

Based on the rBC core mass ($m_{rBC}$) and scattering cross section ($C_s$) of the BC-containing particle derived from the SP2 measurements, the size of the BC-containing particle ($D_p$), including the rBC core and the coating materials, was calculated by Mie theory with a shell-and-core model (Zhang et al., 2016). In Mie calculation, the $D_p$ is retrieved from $C_s$, the size of rBC core ($D_c$) and the refractive indices of the non-BC shell ($RI_s$) and rBC core ($RI_c$).

The $RI_s$ value used in this study are 1.50-0i based on the chemical compositions of coating materials during the campaign period (Fig. S4 and the associated discussion in the supplementary information). In term of $RI_c$, we evaluated the sensitivity of $D_p$ values retrieved by Mie mode to the $RI_c$ values (Fig. S5 and the associated discussion in the supplementary information).

1    In the following calculation, the $RI_c$ of 2.26-1.26i was used (Taylor et al., 2015).

2      The $D_c$ is calculated using the $m_{rBC}$ and rBC core density ($\rho_c$, 1.8 g cm$^{-3}$ used in this study (Cappa et al., 2012)) assuming

3 a void-free sphere for rBC core, as given in Eq. (1). The size distribution of rBC cores under different pollution levels during

4 the campaign period is displayed in Fig. S6.

5 $$\boldsymbol{D_c} = (\frac{6m_{rBC}}{\pi\rho_c})^{1/3}, \quad\quad\quad\quad\quad\quad\quad\quad\quad\quad\quad\quad\quad\quad\quad\quad\quad\quad\quad\quad\quad\quad (1).$$

6      As in previous studies (Liu et al., 2013; Sedlacek et al., 2012; Zhang et al., 2016), the aging degree of BC-containing

7 particles was characterized by the $D_p/D_c$ ratio in this study. Higher $D_p/D_c$ ratios for BC-containing particles indicate higher

8 aging degrees, i.e., more coating materials on the BC surface.

9      In terms of $D_p/D_c$ ratio of BC-containing particles, we focused on the rBC core size ($D_c$) above detection limit of SP2

10 incandescence ($D_c$ >75 nm), while the detection limit of SP2 scattering for the whole particle size ($D_p$) was not considered in

11 this study. If the BC-containing particles with rBC cores larger than ~75 nm is large enough to be detected by SP2 scattering

12 channel, we would calculated their whole particle size ($D_p$) using LEO method based on their scattering signal. If not, we

13 would assume that the $D_p$ was equal to the rBC core size ($D_c$). This assumption might lead to the underestimation of $D_p/D_c$

14 ratio of the BC-containing particles with size above the incandescence limit and blow the scattering limit. To evaluate the

15 uncertainty of $D_p/D_c$ ratio, we calculated the detect efficiency of SP2 scattering (Fig. S7 in the supplementary information). In

16 terms of BC-containing particles with rBC core larger than 75 nm (SP2 size cut for incandescence) observed in our site during

17 the campaign period, most of them (~90-100%, Fig. S7) exhibited particle size (180-500 nm shown in Fig. R8) larger than

18 SP2 size cut for scattering due to large coating materials on rBC cores. This indicated that the uncertainty of $D_p/D_c$ ratio

19 calculated in this study due to mismatch in the SP2 size cut for incandescence vs scattering is no more than 10%. High detection

20 efficiency of SP2 scattering for BC-containing particles observed in our site can be attribute to their large size (180-500 nm,

21 Fig. S8).

22 **2.2.2 BC optical properties**

23 Based on the size information on BC-containing particles (i.e., $D_c$ and $D_p$) obtained from the SP2 measurement (discussed in

24 Sec. 2.2.1), we used Mie theory with a shell-and-core model to retrieve the optical properties of BC-containing particles,

25 including the absorption enhancement ($E_{ab}$) of rBC, the mass absorption cross-section ($MAC$) of BC-containing particles and

26 bare rBC cores, themass scattering cross section of bare BC core ($MSC_{core}$) and the absorption coefficient ($\sigma_{ab}$) of BC-

27 containing particles. The calculation of these parameters is described below.

28      The $E_{ab}$ characterizes the increase in BC light absorption due to the lensing effect of coating materials on the BC surface

29 and is used to quantify the theoretical light absorption capability of BC-containing particles in this study. The $E_{ab}$ is determined

30 by the ratio of the absorption cross section of the entire BC-containing particle ($C_{ab,p}$) to that of bare BC core ($C_{ab,c}$), as

31 expressed in Eq. (2):

1 $$E_{\text{ab}} = \frac{C_{\text{ab,p}}\ (D_c, D_p, RI_s, RI_c)}{C_{\text{ab,c}}(D_c, RI_c)},$$ (2)

2 where $C_{\text{ab,p}}$ is determined by the $D_c$, $D_p$, $RI_s$ and $RI_c$ using Mie calculation, and $C_{\text{ab,c}}$ is determined by the $D_c$ and $RI_c$.

3 The $MAC$ of BC-containing particles ($MAC_p$) and bare rBC cores ($MAC_c$) is defined as the $C_{\text{ab,p}}$ and $C_{\text{ab,c}}$ per unit rBC mass,

4 as Eqs. (3) and (4), respectively:

5 $$MAC_p = \frac{C_{\text{ab,p}}\ (D_c, D_p, RI_s, RI_c)}{m_{rBC}},$$ (3)

6 $$MAC_c = \frac{C_{\text{ab,c}}\ (D_c, RI_c)}{m_{rBC}},$$ (4)

7 The $MSC_{\text{core}}$ is the scattering cross sections of bare rBC cores ($C_{\text{sca,c}}$) per unit rBC mass, as calculated by Eq. (5):

8 $$MSC_{core} = \frac{C_{\text{sca,c}}\ (D_c, RI_c)}{m_{rBC}}.$$ (5)

9 The $\sigma_{\text{ab}}$ of BC-containing particles is calculated based on the $MAC$ and the rBC mass concentration ($C_{\text{rBC}}$) measured by

10 the SP2, as expressed in Eq. (6). The uncertainties of $\sigma_{\text{ab}}$ related to MAC of bare rBC cores from Mie calculation was evaluated

11 in the supplementary information (Fig. S9 and the associated discussion).

12 $$\sigma_{ab,calculated} = MAC_p \times C_{rBC} = MAC_c \times E_{ab} \times C_{rBC},$$ (6).

13 **2.3 BC effective emission intensity**

14 To evaluate the impact of regional transport on BC-containing particles, we used a variant of the "effective emission intensity"

15 (EEI) defined by Lu et al. (2012) to quantify the amounts of BC over the observation site from different source regions. In this

16 study, the spatial origin of the BC observed at our site was divided into local sources in Beijing and regional sources in other

17 areas (i.e., Hebei, Tianjin, Shanxi and Inner Mongolia, Fig. S1). The EEI takes into account emission, transport, hydrophilic-

18 to-hydrophobic conversion, and removal processes (i.e., dry and wet deposition) of BC throughout the whole atmospheric

19 transport process from the origin of the BC emission to the receptor site. A novel back-trajectory approach was developed by

20 Lu et al. (2012) to calculate EEI values.

21 In this study, the back-trajectory analysis was performed by the Hybrid Single-Particle Lagrangian Integrated Trajectory

22 (HYSPLIT) model to obtain the transport pathways of BC to the observation site (40º00'17" N, 116º19'34" E) during the

23 campaign period (November 17-30, 2014). The 72-h back-trajectory at 100 m at every hour was calculated with the

24 meteorological fields of NCEP GDAS at a 1º×1º resolution. An anthropogenic BC emission inventory of China in the year

25 2012 at a resolution of 0.25º×0.25º was used to support the back-trajectory analysis. The gridded BC emission data are from

26 the Multi-resolution Emission Inventory for China (MEIC) developed by Tsinghua University (http://www.meicmodel.org).

27 We calculated the EEI of BC at a resolution of 0.25º×0.25º based on the algorithm developed by Lu et al. (2012). Following

28 a trajectory $l$ at every hour, the fresh BC emitted from a series of spatial grids in sequence (i.e., $l_1$, $l_2$, …, $l_{i,…}$) are transported

29 to the receptor grid (i.e., $l_n$). The EEI of trajectory $l$ at the surface grid point $i$ ($EEI_{i,l}$) was determined by Eq. (7):

30 $$EEI_{i,l} = E_i \times TE_{i,l},$$ (7)

1    where $E_i$ is the BC emission at the surface grid point $i$, and $TE_{i,l}$ represents the BC transport efficiency of trajectory $l$ from the

2    grid point $i$ to the receptor site, as calculated by Eqs. (1)-(4) in Lu et al. (2012).

3        The total EEI of trajectory $l$ characterizes the total amount of BC transported to the observation site at every hour, expressed

4    as Eq. (8):

5    $EEI_{total} = \sum_{i=1}^{n} EEI_{i,l},$ (8).

6    **2.4 BC radiative efficiency**

7    In this study, we use a parameter of the simple forcing efficiency (*SFE*) to roughly evaluate the radiative forcing of BC-

8    containing particles. The *SFE* is defined as normalized radiative forcing by BC mass, which is wavelength-dependent (Bond

9    and Bergstrom, 2006; Chen and Bond, 2010; Chylek and Wong, 1995; Saliba et al., 2016). The wavelength-dependent *SFE*

10   for BC-containing particles is determined by Eq. (9):

11   $\frac{dSFE}{d\lambda} = -\frac{1}{4}\frac{dS(\lambda)}{d\lambda}\tau_{atm}^2(\lambda)(1 - F_c) \times [2(1 - \alpha_s)^2\beta(\lambda) \cdot MSC_{core}(\lambda) - 4\alpha_s \times MAC(\lambda)],$ (9)

12   in which a wavelength ($\lambda$) of 550 nm is used in this study; dS ($\lambda$)/d$\lambda$ is the spectral solar irradiance, the value of which is from

13   the ASTM G173-03 Reference Spectra (1.86 W m$^{-2}$ nm$^{-1}$ at 550 nm); and the parameters $\tau_{atm}$, $F_c$, $\alpha_s$ and $\beta$ are the atmospheric

14   transmission (0.79), cloud fraction (0.6), urban surface albedo (0.15) and backscatter fraction (0.17), respectively (Jeong et al.,

15   2013; Chen and Bond, 2010; Park et al., 2011; Saliba et al., 2016).

16   **3 Results**

17   **3.1 Light absorption of BC-containing particles during the campaign period**

18   Figure 1 shows the time series of the PM$_1$ and rBC mass concentration, the diameter of BC-containing particles ($D_p$) and the

19   measured and calculated light absorption coefficient ($\sigma_{ab}$) at 880 nm. During the campaign period, four episodes with different

20   PM$_1$ evolution processes (Fig. 1a) were observed: November 18-21, November 23-24, November 25-26 and November 28-

21   30. The hourly PM$_1$ mass concentration ranged from 3.5-275 μg m$^{-3}$, with an average value of 91 μg m$^{-3}$ during the observed

22   period. The rBC mass concentration accounted for ~5% of PM$_1$. The diameter of BC-containing particles ($D_p$) including rBC

23   cores and coating materials shown in Figure 1(b) exhibited an excellent temporal coherence with the rBC mass concentration.

24   Figure 1(b) shows that the number distribution of $D_p$ for BC-containing particles exhibited a peak at 180-320 nm, significantly

25   larger than the peak value ($D_c$ of ~95 nm) for number size distribution of bare rBC cores (Fig. S5a) due to larges of coating

26   materials on BC surface. The size information (namely entire particle size ($D_p$) and rBC core size ($D_c$)) of BC-containing

27   particles observed in our study was consistent with those ($D_p$ of ~200-300 nm and $D_c$ of ~70-100 nm) in previous studies in

28   China (Gong et al., 2016; Huang et al., 2012; Wang et al., 2014). Moreover, the $D_p$ exhibited sustained growth from ~180 nm

29   to ~400 nm during a pollution episode, which could be a consequence of the increase in either $D_c$ or coating materials, or both.

1    Figure S6a shows a slight change in $D_c$ with pollution development. However, the coating thickness of BC-containing particles

2    increased with $PM_1$ concentration (Fig. S10a). Therefore, the sustained growth of $D_p$ during a pollution episode was dominated

3    by more coating materials under more polluted conditions. Figure S10 shows the simultaneous increase in the rBC mass

4    concentration and the amount of coating materials on the BC surface, which could significantly enhance the light absorption

5    of BC-containing particles. Figure S11 shows that the measured absorption coefficient ($\sigma_{ab, measured}$) at 880 nm (dominated by

6    BC component at this wavelength (Drinovec et al., 2015)) for the aerosol particles measured by the AE33 exhibited an 18-fold

7    increase in conjunction with an increase in the $PM_1$ concentration from ~10 μg m$^{-3}$ to ~230 μg m$^{-3}$.

8       To valid SP2 measurements and Mie calculation used in this study, we compared the calculated light absorption coefficient

9    ($\sigma_{ab, calculated}$) of BC-containing particles using Eq. (6) with the measured light absorption coefficient ($\sigma_{ab, measured}$) from AE33,

10   as shown in Fig. 1c. The $\sigma_{ab, calculated}$ values for BC-containing particles showed an excellent agreement with the $\sigma_{ab, measured}$

11   values measured by the AE33, with a difference of ~10% ($R^2$=0.98). The difference was dominated by the uncertainties from

12   compensation algorithm used in the AE33 measurements (~15%, details shown in Fig. S2 and the associated discussion in the

13   supplementary information) and Mie calculation (10-20%, Fig. S4, Fig. S5 and Fig. S9 and the associated discussion in the

14   supplementary information). The uncertainty evaluation revealed that the difference between $\sigma_{ab,calculated}$ and $\sigma_{ab,cmeasured}$ (~10%)

15   shown in Fig. 1c is reasonable. The comparison between the $\sigma_{ab, calculated}$ and $\sigma_{ab, measured}$ values implied that the optical properties

16   (i.e., $\sigma_{ab}$, $MAC$ and $E_{ab}$) of the BC-containing particles derived from Mie calculation combining with SP2 measurement data

17   (i.e., rBC concentrations, $D_p$ and $D_c$) were reliable in our case.

## 3.2 Enhancement of the theoretical light absorption capability of black carbon associated with air pollution

### 3.2.1 The $D_p$/$D_c$ ratio and calculated $E_{ab}$ under different $PM_1$ concentrations

20   Previous theoretical studies reported that the coating materials on the BC surface can significantly enhance the light absorption

21   of BC via the lensing effect (Fuller et al., 1999; Jacobson, 2001; Lack and Cappa, 2010; Moffet et al., 2009). In other words,

22   the aging degree of BC-containing particles (characterized by the $D_p$/$D_c$ ratio in this study) determines their light absorption

23   capability (characterized by the calculated $MAC$ and $E_{ab}$ in this study). However, whether and how the aging degree and light

24   absorption capability of BC-containing particles will change under different pollution levels remains unclear. During the

25   campaign period, we found that the mass-averaged values of $D_p$/$D_c$ ratio and calculated $E_{ab}$ of BC-containing particles

26   increased with increasing air pollution levels.

27       Figure 2a shows the $D_p$/$D_c$ ratio and calculated $E_{ab}$ of BC-containing particles with rBC cores at 75-300 nm under different

28   $PM_1$ concentrations in the range of 1.2-3.5 and 1.3-3.1, respectively. In terms of BC-containing particles with a certain rBC

29   core size, their $D_p$/$D_c$ ratio and calculated $E_{ab}$ were greater under higher $PM_1$ concentrations, which could be attributed to more

30   coating materials on BC surface under more pollution environment. The increase of both primary and secondary components

31   under more polluted conditions was favorable to BC aging by coagulation and condensation, which happen mostly between

32   BC and non-BC species. On average (i.e., mass-weighted mean across rBC core size larger than ~75 nm), the $D_p$/$D_c$ and

calculated $E_{ab}$ for observed BC-containing particles in SP2 under different $PM_1$ concentrations during the campaign period varied in the range of 1.6-2.2 and 1.6-2.0, respectively (Fig. 2b). Correspondingly, the mass-averaged values of the $D_p/D_c$ and calculated $E_{ab}$ of BC-containing particles increased by ~33% and ~18%, respectively, with increasing $PM_1$ concentrations from ~10 μg m$^{-3}$ to ~230 μg m$^{-3}$.

Figure 3 shows the increase of the $D_p/D_c$ ratio and calculated $E_{ab}$ ($IR_{Dp/Dc}$ and $IR_{Eab}$, respectively) for BC-containing particles with increasing $PM_1$ concentrations form 10 μg m$^{-3}$ to 230 μg m$^{-3}$ as a function of rBC core size. Based on the $D_p/D_c$ ratio and calculated $E_{ab}$ of BC-containing particles with size-resolved rBC cores in SP2 measurement under different $PM_1$ concentration (shown in Fig. 2a), we can obtain the measured $IR_{Dp/Dc}$ and $IR_{Eab}$ as a function of rBC core size. When $PM_1$ concentration increasing from ~10 μg m$^{-3}$ to ~230 μg m$^{-3}$ during the campaign period, the $D_p/D_c$ ratio and calculated $E_{ab}$ of BC-containing particle with rBC cores at 75-200 nm increased by 28-48% and 13-36%, respectively. The size-dependent increase of $D_p/D_c$ ratio and calculated $E_{ab}$ associated with air pollution indicated that the aging process of smaller rBC was relatively more sensitive to air pollution levels. This could be attributed to the fact that the condensational growth associated with air pollution due to the formation of secondary components is more effective for smaller particles in terms of increasing the diameter (Metcalf et al., 2013).

Meanwhile, following a semiquantitative analysis using in Metcalf et al. (2013), we calculated the $IR_{Dp/Dc}$ and $IR_{Eab}$ based on diffusion-controlled growth law (Seinfeld and Pandis 2006).

According to the diffusion-controlled growth law (Seinfeld and Pandis 2006), the evolution of the size of BC-containing particles ($D_p$) is shown:

$$\frac{dD_P}{dt} = \frac{A}{D_P} \tag{10}$$

in which, $\frac{dD_P}{dt}$ represents the diffusion-controlled growth rate; A is a parameter. Integrating Eq. (10) with $D_p$ ($t = 0$) = $D_c$:

$$D_p^2 = D_c^2 + 2At = D_c^2 + B \tag{11}$$

in which, $D_c$ is rBC core diameter; $B$ (i.e., $2At$) is a parameter, varying under different $PM_1$ concentrations.

Following Eq. (11), the $D_p/D_c$ ratio is given:

$$\frac{D_p}{D_c} = (\frac{B}{D_c^2} + 1)^{1/2} \tag{12}$$

where the parameter $B$ is determined by the value of the measured $D_p/D_c$ ratio with $D_c$ of 160 nm under different $PM_1$ concentrations.

The increase ratio of the $D_p/D_c$ ($IR_{Dp/Dc}$) for BC-containing particles with $PM_1$ concentration increasing from 10 μg m$^{-3}$ to 230 μg m$^{-3}$ can be calculated by Eq. (13):

$$IR_{Dp/Dc} = \frac{(\frac{D_p}{D_c})_{230} - (\frac{D_p}{D_c})_{10}}{(\frac{D_p}{D_c})_{10}} = \frac{(\frac{B_{230}}{D_c^2} + 1)^{1/2} - (\frac{B_{10}}{D_c^2} + 1)^{1/2}}{(\frac{B_{10}}{D_c^2} + 1)^{1/2}} \tag{13}$$

1    where $(\frac{D_p}{D_c})_{230}$ and $(\frac{D_p}{D_c})_{10}$ represent the $D_p/D_c$ ratio when $PM_1$ concentrations are 230 µg m$^{-3}$ and 10 µg m$^{-3}$, respectively; $B_{230}$

2    and $B_{10}$ are parameter $B$ with $PM_1$ concentrations of 230 µg m$^{-3}$ and 10 µg m$^{-3}$, respectively.

3        The increase ratio of calculated $E_{ab}$ ($IR_{Eab}$) for BC-containing particles with $PM_1$ concentration increasing from 10 µg m$^{-3}$

4    to 230 µg m$^{-3}$ can be derived based on $E_{ab}=k\times(D_p/D_c)$, as expressed in Eq. (5):

$$IR_{Dp/Dc} = \frac{(\frac{D_p}{D_c})_{230} - (\frac{D_p}{D_c})_{10}}{(\frac{D_p}{D_c})_{10}} = \frac{k_{230} \times (\frac{B_{230}}{D_c^2}+1)^{1/2} - k_{10} \times (\frac{B_{10}}{D_c^2}+1)^{1/2}}{k_{10} \times (\frac{B_{10}}{D_c^2}+1)^{1/2}} \qquad (14)$$

6        We compared the calculated $IR_{Dp/Dc}$ and $IR_{Eab}$ based on Eqs. (13) and (14) with those from SP2 measurements, as shown

7    in Fig.3. The agreement indicated that the increase of the $D_p/D_c$ and $E_{ab}$ for BC-containing particles with increasing $PM_1$

8    concentrations follow the diffusion-controlled growth law.

9    **3.2.2 Changing rate of the theoretical light absorption capability of black carbon**

10    Figure 4a explores the relationship between the changing rate of calculated $E_{ab}$ ($k_{Eab}$) and the changing rates of $PM_1$

11    concentrations ($k_{PM1}$) with pollution development. Linear relationships were estimated, i.e., $k_{Eab} \approx 0.051\ k_{PM1}$, revealing that

12    rapid increases in air pollution levels lead to rapid increases in BC light absorption capability. When the $PM_1$ concentration

13    exhibited a sharp increase related to an extreme haze episode (Zheng et al., 2015), the increase in BC light absorption capability

14    was dramatic. Figure 4b shows frequency distribution of $k_{Eab}$, $k_{PM1}$, and $k_{Eab}/k_{PM1}$ ratio. During the campaign period, most of

15    $k_{Eab}$ and $k_{PM1}$ values were in the range of -50%-50% h$^{-1}$ and -4%-4% h$^{-1}$, respectively, revealing a lower changing rate for BC

16    aging than that for $PM_1$ concentration. The peak value of frequency distribution of $k_{Eab}$ was around zero, indicating the BC-

17    containing particles were shrinking as often as they were growing. The $k_{Eab}/k_{PM1}$ ratio characterized the sensitivity of the change

18    of calculated $E_{ab}$ with changing $PM_1$ concentrations. The frequency distribution of $k_{Eab}/k_{PM1}$ ratio showed that ~60% values

19    were in the range of 0-1, with a peak value around 0.05. Smaller values of $k_{Eab}/k_{PM1}$ ratio indicated that the change of calculated

20    $E_{ab}$ was not sensitive to variations in $PM_1$ concentrations .The growth rate of $E_{ab}$ (for BC samples with $k_{Eab}>0$: 0.1-7.3% h$^{-1}$)

21    observed at our study was consistent with the BC aging rate (0.2-7.8% h$^{-1}$) in previous studies (Cheng et al., 2012; Moteki et

22    al., 2007; Shiraiwa et al., 2007). Moreover, we found that the growth rate of $E_{ab}$ decreased with increasing $PM_1$ mass

23    concentrations (Fig. S12a), indicating that the increase in the theoretical light absorption capability of BC-containing particles

24    slowed with further pollution development. This can be explained by larger BC-containing particles when $PM_1$ concentration

25    is higher (Fig. S12b). The net change in diameter for a given amount of material deposited decreases with increasing particle

26    size due to surface-to-volume scaling, which would expect the growth rate of particles to decrease with increasing $PM_1$

27    concentration and thus the $k_{Eab}$ would also decrease (Fig. S12a).

28        The evolution of theoretical light absorption of BC with pollution levels depends on the change in both rBC mass

29    concentrations and calculated $E_{ab}$. Figure S13 shows markedly smaller $k_{Eab}$ than $k_{rBC}$ ($k_{Eab} \approx 0.027\ k_{rBC}$), indicating the change

30    of calculated $E_{ab}$ was significantly slower than that of rBC mass concentrations under different pollution levels. Due to less

1  sensitive for calculated $E_{ab}$ to change in air pollution levels compared with that for rBC mass concentrations, some previous

2  measurements (McMeeking et al., 2011; Ram et al., 2009; Wang et al., 2014b; Andreae, et al., 2008) would not have been able

3  to discern a difference of $E_{ab}$ easily among different pollution levels and thus just focus on the change of BC mass

4  concentration. This would lead to uncertainties in estimation of BC light absorption. In our case, we found the mass-weighted

5  average of calculated $E_{ab}$ increased by ~18% with $PM_1$ concentration increasing from ~10 μg m$^{-3}$ to ~230 μg m$^{-3}$ (Fig. 2b). If

6  the increase in calculated $E_{ab}$ of BC with $PM_1$ increase was neglected in this study, the theoretical light absorption of BC-

7  containing particles would be underestimated by ~18% under polluted conditions.

8  **3.3 Contribution of regional transport**

9  BC aging in the atmosphere, namely BC internally mixing with other aerosol components, is associated with atmospheric

10  transport (Gustafsson and Ramanathan, 2016). In Beijing, the rapid increase in aerosol particle concentrations during pollution

11  episodes is most likely caused by regional transport of polluted air mass (Yang et al., 2015; Zheng et al., 2015). Therefore,

12  regional transport of pollution may play an important role in the enhancement of BC light absorption capability associated

13  with air pollution. In this study, we used the EEI analysis (Lu et al., 2012) to explore the effects of regional transport on the

14  increase in theoretical light absorption capability of BC with increasing pollution levels.

15  Figure 5 shows the spatial distribution (0.25°×0.25°) of the EEI for BC transported to the observation site under different

16  pollution levels (i.e., clear, slightly polluted and polluted periods) during the campaign period. The spatial origin of the BC

17  observed at our site varied significantly among the different pollution periods. In this study, the spatial origin of total BC in

18  the site was classified into local Beijing and other regions (i.e., outside of Beijing, considered as regional origins in this study).

19  Noted that the local region (i.e., Beijing) defined in this study is smaller than areas outside Beijing (e.g., Hebei, Tianjin, Shanxi

20  and Inner Mongolia (Fig. S1)). Table 1 lists the contribution of BC from regional origins (i.e., $EEI_{ousiede}/EEI_{total}$ ratio). During

21  polluted period, the contributions of BC from regional origins was ~63%, larger than that from local Beijing (~37%). This was

22  partly due to comparing the contributions from a small region (Beijing) and a large region (outside of Beijing). In this study,

23  we focus on comparing the contributions of BC from outside of Beijing (considered as regional origins in this study) among

24  different pollution levels (i.e., clean, slight polluted and polluted period). The BC from regional origins (i.e., outside of Beijing)

25  accounted for ~21%, 39% and ~63% of total BC amount in the site during the clean, slightly polluted and polluted periods,

26  respectively. This revealed that the regional contribution to BC over Beijing increased as the air pollution levels increased.

27  Due to the increase of the regional contribution, the total BC amount transported to the observation site, characterized by

28  the EEI $(EEI_{total})$ in this study, increased under more polluted condition. Table 1 shows that the $EEI_{total}$ was 4.6 times higher

29  during the polluted period than during the clean period, revealing that polluted air mass brought more BC to Beijing. BC

30  concentration in the site strongly depends on both total BC amount (transported from local Beijing and other regions,

31  characterized by $EEI_{total}$ in this study) and local meteorology. Table 1 shows that the BC concentrations from the clean period

32  to the polluted period increase by ~7.4 times. The increase of $EEI_{total}$ (~4.6 times) accounted for ~62% the increase in BC mass

concentrations (~7.4 times). This indicated that the adverse local meteorology contributed ~38% of the increase in BC mass concentration in the site from the clean period to the polluted period. Compared with regional transport, less effect of adverse local meteorology might be attributed to relatively small areas defined as the local region (i.e., Beijing) in this study. Polluted events in China always occur over a large region, e.g., North China Plain (Yang et al., 2017; Zheng et al., 2015). For our case, the adverse meteorology during polluted days in the whole large region including Beijing and other areas can lead to the increase of pollutants and then more transport of pollutants into Beijing. Yang et al. (2017) found that the increases in BC concentration under polluted conditions over the North China Plain (including Beijing and other adjacent areas) is dominated by its local emissions due to adverse meteorology.

Under different pollution levels, regional transport not only influenced the BC mass concentrations but also the BC aging process and timescale. Table 1 shows that the mass-average value of the $D_p/D_c$ ratio of BC-containing particles at our site was ~2.04 during the polluted period, significantly higher than that observed during the clean period (~1.62) and slightly polluted period (~1.81). On one hand, under more polluted conditions, more BC-containing particles in Beijing were from regional sources and thus had undergone a longer aging time during the transport than the BC from local sources in Beijing. On the other hand, compared with the BC carried in the clean air mass from the northwest of Beijing during the clean period (Fig. 5a), the BC-containing particles in the polluted air mass undergoing regional transport from the region south of Beijing (i.e., Hebei, one of the most polluted provinces in China with high pollutant emission) during the polluted periods (Fig. 5c). Peng et al. (2015) pointed out higher BC aging rates under more polluted environments, indicating that BC-containing particles passing though polluted regions would show higher aging rates during atmospheric transport than that from clean regions. The mass-average values of calculated $E_{ab}$ for BC-containing particles observed at our site were ~1.66, ~1.81 and ~1.91 during the clean, slightly polluted and polluted periods, respectively (Table 1), showing that the theoretical light absorption capability of BC-containing particles observed at our site increased with increasing regional contributions. Our results demonstrated the importance of regional transport in the enhancement of BC light absorption capability associated with air pollution.

To further explore the importance of aging during regional transport, its contributions were compared with those of local chemical processes with respect to increases in $D_p/D_c$ ratio and theoretical light absorption capability of BC-containing particles associated with air pollution. Considering the formation of coating materials on BC surface is dominated by photochemical oxidation (Metcalf et al., 2013; Peng et al., 2015), we evaluated the contribution of local photochemical production by the changes of $O_3$ concentrations in the atmosphere. On the other hand, the changes in the amount of BC from regional transport was characterized by variation of $EEI_{total}$, which was used to evaluate the contributions of regional transport to BC aging.. Figure 5a shows that the $EEI_{total}$ per hour exhibited a temporal coherence with the mass-averaged values of the $D_p/D_c$ ratio and calculated $E_{ab}$ of BC-containing particles. In contrast, the $O_3$ concentrations showed a different temporal trend. When $PM_1$ concentrations were higher than ~120 μg m$^{-3}$, $O_3$ concentrations decreased to ~2 ppb. Zheng et al. (2015) has demonstrated the weakened importance of photochemistry in the production and aging of secondary aerosols in Beijing under polluted conditions due to decrease of oxidant concentrations. This indicated that the photochemical processing in BC aging may be weakened under higher polluted levels (i.e., $PM_1 > 120$μg m$^{-3}$). Noted that photochemical processing is not the only

1  possible pathway in BC aging process and other pathways were not discussed in this study. The local aging process of BC

2  might be enhanced by other pathways. For example, high concentrations of aerosols under polluted environment may

3  compensate the adverse photochemical conditions for BC aging. In summary, the increases in the aging degree and theoretical

4  light absorption capability of BC-containing particles with increasing air pollution were more likely caused by aging during

5  regional transport than by local photochemical production.

6      According to the evolution of the $EEI_{total}$ values and $O_3$ concentrations with increasing air pollution levels (Fig. 5b1 and

7  Fig.5b2), we separated the pollution levels into two periods. When $PM_1$ concentrations were lower than ~120 μg m$^{-3}$ and rBC

8  mass concentrations were lower than ~6 μg m$^{-3}$, the normalized $EEI_{total}$ increased from ~3 to ~18 with increasing air pollution

9  levels, and the $O_3$ concentrations decreased from ~20 ppb to ~2 ppb, indicating enhanced regional contributions and weakened

10  local photochemical production at observation site. In this period, Fig. 5b3 and Fig. 5b4 show that the mass-averaged values

11  of calculated $E_{ab}$ and the $D_p/D_c$ ratio of BC-containing particles increased from ~1.6 to ~1.9 and from ~1.6 to ~2.0, respectively,

12  with the increase in the normalized $EEI_{total}$ (from ~3 to 18) and the decrease in the $O_3$ concentrations (from ~20 to 2 ppb).

13  Therefore, in terms of the increase in the BC light absorption capability with increasing air pollution levels, this period (i.e.,

14  conditions of $PM_1$<120 μg m$^{-3}$ and rBC < 6 μg m$^{-3}$) represented a regional transport-controlled period. The increase in

15  calculated $E_{ab}$ of BC-containing particles (~1.6-1.9) during this regional transport-controlled period accounted for ~75% of

16  the increase in calculated $E_{ab}$ (~1.6-2.0) with increasing air pollution during the whole campaign period. Therefore, the aging

17  process during the regional transport dominated the increase in the theoretical light absorption capability of BC-containing

18  particles in Beijing during the campaign period. Another period is defined by $PM_1$ concentrations of more than ~120 μg m$^{-3}$

19  and rBC mass concentrations of more than ~6 μg m$^{-3}$, during which both the $EEI_{total}$ and $O_3$ concentrations showed slight

20  changes with increasing air pollution levels. In this period, the increase in calculated $E_{ab}$ of BC-containing particles (from ~1.9

21  to ~2.0) might be attributed to local heterogeneous chemical production in Beijing.

22  **3.4 Implications for BC radiative forcing**

23  The increase in BC light absorption capability with increasing air pollution levels suggests that greater solar absorption (i.e.,

24  direct radiative forcing (DRF)) by atmospheric BC occurs under more polluted conditions. The DRF of atmospheric BC-

25  containing particles depends not only on the BC mass concentrations but also on the BC forcing efficiency, which strongly

26  depends on the light absorption capability of BC-containing particles. In this study, the forcing efficiency of BC-containing

27  particles was estimated based on a simple radiation transfer model (Eq. (9)). Figure 6 shows that with increasing pollution

28  levels (i.e., $PM_1$ increasing from ~10 μg m$^{-3}$ to ~230 μg m$^{-3}$) during the campaign period, the mass-averaged values of

29  calculated MAC at 550 nm for BC-containing particles increased from ~11 m$^2$ g$^{-1}$ to ~14 m$^2$ g$^{-1}$, which resulted in the SFE of

30  BC-containing particles increasing from ~0.7 m$^2$ g$^{-1}$ nm$^{-1}$ to ~0.9 m$^2$ g$^{-1}$ nm$^{-1}$. Meanwhile, the DRF of BC-containing particles

31  increased from ~0.51 W m$^{-2}$ to ~0.61 W m$^{-2}$ (Fig. 7c), revealing the importance of BC in terms of solar absorption under more

32  polluted conditions. In this case, the failure to consider the increase in BC light absorption capability with increasing air

pollution levels may cause underestimation of the radiative forcing of BC-containing particles in Beijing under polluted conditions. Noted that DRF calculation shown in Fig .7c did not consider the changes of total BC amount to point out the effect of BC light-absorption capability on DRF under different $PM_1$ concentrations.

Fig. 7c shows the DRF of BC increased by ~18% during the polluted period compared with that during the clean period. Meanwhile, the BC mass concentration increased by ~7 times (Table 1). If assuming the DRF of BC during the clean period to be ~0.5 W m$^{-2}$ based on calculation shown in Fig. 7c, it would increase to ~4 W m$^{-2}$ under polluted conditions, taking the increase in both of the mass concentration and theoretical absorption capability of BC.

The enhanced climate effects of BC aerosols in Beijing could be taken to be representative of polluted regions in China. Previous measurements of BC aerosols in China (Zheng et al., 2015; Wang et al., 2014b; Zhao et al., 2017; Gong et al., 2016; Huang et al., 2013; Andreae et al., 2008; Zhang et al., 2014) showed that the BC mass concentrations in different regions (e.g., Beijing, Xi'an, Nanjing, Shanghai and Guangzhou) reached values of ~10-50 µg m$^{-3}$ during polluted periods (Table S2), similar to our measurements. Therefore, our BC aerosol observations in Beijing were not a special case. In China, high concentrations of BC aerosols under polluted conditions always occur on a regional scale due to intense BC emissions (Zhang et al., 2009; Li et al., 2017) and significant regional transport (Zheng et al., 2015; Wang et al., 2014a; Zhao et al., 2013). Our findings in Beijing can provide some implication in the difference of BC radiative forcing in other regions among different air pollution levels.

**4 Discussion: breaking the amplification effect by emission control**

Our results reveal that under more polluted environment, the BC-containing particles are characterized by more BC mass concentrations and more coating materials on BC surface and therefore higher light absorption capability. As shown in Fig. 8, this amplification effect on BC light absorption associated with air pollution is caused by increasing BC concentration and at the same time enhanced light absorption capability of BC-containing particles by more coating production in the more polluted air. Variation of both the mass concentration and light absorption capability of BC associated with air pollution strongly depend on the air pollutant emission (e.g., BC, SO2, NO$_x$ and VOC). Under polluted environment, polluted air mass from high emission areas not only brings more BC, but also more coating materials on BC surface due to more precursors of secondary components.

Air pollution control measures may, on the other hand, break this amplification effect by reducing BC concentration and at the same time lowering the light absorption capability of BC-containing particles by slowing down the coating processes with a cleaner air (Fig. 7). Take air pollution controls during the 2014 Asia-Pacific Economic Cooperation meeting (APEC) in Beijing, China as an example, we found that as a result of emission controls on local Beijing and areas adjacent to Beijing (i.e., Hebei, Tianjin, Shanxi, Henan, Shandong and Inner Mongolia), light absorption of BC-containing particles decreased significantly during APEC compared to that of before APEC under polluted conditions (Zhang et al., 2018). This is not only contributed by a reduction of BC mass concentration, but also by lower light absorption capability of BC-containing particles

1 with less coating materials on BC surface in cleaner atmosphere conditions, indicating that synergetic emission reduction of

2 multi-pollutants could achieve co-benefits of both air quality and climate.

3 **5 Conclusions**

4 The light absorption of BC-containing particles depends not only on the BC mass concentration but also on their light

5 absorption capability (characterized by the calculated MAC and $E_{ab}$ in this study). In this work, we investigated the difference

6 of theoretical light absorption capability of BC under different air pollution conditions. During an intensive field measurement

7 campaign in Beijing, China, we found that with increasing pollution levels, the increase in BC mass concentration was always

8 accompanied by an increase in the theoretical light absorption capability of BC, resulting an amplification effect on the light

9 absorption of the ambient BC-containing particles. During the campaign period, the hourly values of mass-weighted averages

10 of the $D_p/D_c$ ratio and calculated $E_{ab}$ for BC-containing particles was in the range of 1.5-2.3 and 1.5-2.0, respectively. When

11 PM$_1$ concentration increased from ~10 μg m$^{-3}$ to ~230 μg m$^{-3}$ accompanied with the rBC mass concentration in the range of

12 ~0.7-11 μg m$^{-3}$, the mass-weighted averages of the $D_p/D_c$ ratio and calculated $E_{ab}$ values increased by ~33% and ~18%,

13 respectively. The increase in BC light absorption capability associated with increasing air pollution can be explained by the

14 increase in coating materials on the BC surface under more polluted conditions. Moreover, the increase of the $D_p/D_c$ ratio and

15 calculated $E_{ab}$ with increasing air pollution levels was size-dependent, namely more increase was exhibited for smaller rBC

16 cores. This indicated that the aging degree and light absorption capability of smaller rBC was more sensitive to air pollution

17 levels. Using a semiquantitative analysis method based on the diffusion-controlled growth law (Seinfeld and Pandis 2006), we

18 also calculated the theoretical increase in the $D_p/D_c$ ratio and calculated $E_{ab}$ with increasing pollution levels for BC-containing

19 particles with size-resolved rBC cores. The agreement between the measured and theoretical increase in the $D_p/D_c$ ratio and

20 $E_{ab}$ indicated the increase of coating materials on BC surface with increasing PM$_1$ concentrations following the diffusion-

21 controlled growth law.

22 The relationships between the changing rate of calculated $E_{ab}$ ($k_{Eab}$) with air pollution development and that of the PM$_1$ and

23 rBC concentrations ($k_{PM1}$ and $k_{rBC}$, respectively) were estimated: $k_{Eab} \approx 0.051\ k_{PM1}$, and $k_{Eab} \approx 0.027\ k_{rBC}$. During the campaign

24 period, $k_{Eab}$ values were in the range of -4%-4% h$^{-1}$, with a peak of frequency distribution around zero, indicating that the BC-

25 containing particles were shrinking as often as they were growing. The frequency distribution of $k_{Eab}/k_{PM1}$ ratio showed that a

26 peak value around 0.05, revealing that the change of calculated $E_{ab}$ was not sensitive to variations in PM$_1$ concentrations.

27 Although the changing rate of the BC light absorption capability was significantly lower than that of the BC mass

28 concentration, the effect of enhanced BC light absorption capability on the light absorption of ambient BC-containing particles

29 under polluted conditions is not negligible. In our case, if we had not considered the increase in the theoretical light absorption

30 capability of BC with increasing air pollution during the campaign period, the theoretical light absorption of BC-containing

31 particles under polluted conditions would have been underestimated by ~18%.

32 The increase in BC light absorption capability with increasing pollution levels in Beijing was controlled by aging during

1    regional transport. The EEI analysis showed that ~63% of the BC observed at our site was transported from regional sources

2    (i.e., areas outside of Beijing) during the polluted period, whereas the regional contributions were significantly lower (~21%)

3    during the clean period. More BC in more polluted air from regional transport could lead to a higher local BC concentration

4    in Beijing. Not only more BC but also more coatings are carried into Beijing by more polluted regional air mass (Fig. 8 (a)),

5    which can be explained by more coating precursors (e.g. $SO_2$, $NO_x$ and VOC) in a more polluted air. Moreover, we separated

6    the change of the $D_p/D_c$ ratio and theoretical light absorption capability of BC associated with air pollution into regional

7    transport-controlled period (i.e., $PM_1 < 120$ μg m$^{-3}$ and BC $< 6$ μg m$^{-3}$) and local chemistry-controlled period (i.e., $PM_1 > 120$

8    μg m$^{-3}$ and BC $> 6$ μg m$^{-3}$). In the regional transport-controlled period, the mass-averaged values of $D_p/D_c$ and calculated $E_{ab}$

9    of BC-containing particles in Beijing increased from ~1.6 to ~2.2 and from ~1.6 to ~2.0, respectively, with increasing pollution

10    levels. The further increase in mass-averaged values of $D_p/D_c$ (~ 2.0 to ~2.2) and calculated $E_{ab}$ (~1.9 to ~2.0) associated with

11    air pollution is harder and is mostly likely attributed to local chemical production. Therefore, we attributed ~75% of the

12    increase in theoretical light absorption capability of BC with increasing air pollution during the campaign period to aging

13    during regional transport, demonstrating the regional transport has an important influence on the variations of light absorption

14    capability of BC-containing particles in Beijing under different pollution levels.

15    Due to the increase in BC light absorption capability with increasing air pollution levels, stronger forcing efficiency of the

16    BC-containing particles was found under more polluted conditions. During the campaign period, the BC forcing efficiency

17    increased by ~18% with $PM_1$ increasing from 10μg m$^{-3}$ to 230 μg m$^{-3}$. Considering the increasing in both of BC forcing

18    efficiency and BC mass concentration, the DRF values of ambient BC-containing particles could increase from ~0.5 W m$^{-2}$

19    during the clean period to ~4 W m$^{-2}$ under polluted conditions. The results identified that BC in more polluted environment

20    exhibited a larger DRF radiative forcing, which was caused not only by the increase of BC mass concentrations but also by

21    the enhancement of BC light absorption capability.

22    The amplification effect on BC DRF due to the increase of BC light absorption capability introduced in this work not only

23    concerns in Beijing but is also likely to operate in other polluted regions in China The amplification effect not only could

24    increase the direct contribution of BC to air pollution and climate change due to more light absorption, but also would enhance

25    the indirect contribution by stronger aerosol-meteorology and aerosol-climate feedbacks. Our finds in this work can provide

26    some implication in the difference of BC-related effect on air quality and climate under different air pollution conditions (e.g.,

27    air clean and putted environment) due to change in BC light absorption capability associated with air pollution.

28    The air pollution control may break the amplification effect by reducing BC concentration and at the same time lower the

29    light absorption capability of BC-containing particles by slowdown the coating processes with a cleaner air. Thereby, breaking

30    the amplification effect by emission control would achieve a co-benefit effect by simultaneous mitigation of air pollution and

31    climate change. Further study will focus on if and how emission reduction of BC and other pollutants in China will break the

32    amplification effect.

1 **Acknowledgments**

2 This work was supported by the National Natural Science Foundation of China (41625020, 41571130032 and 91644218) and

3 the Guangdong "Pearl River Talents Plan" (2016ZT06N263).

4 **References**

5 Andreae, M. O., Schmid, O., Yang, H., Chand, D., Zhen Yu, J., Zeng, L.-M., and Zhang, Y.-H.: Optical properties and chemical

6 composition of the atmospheric aerosol in urban Guangzhou, China, *Atmos. Environ.*, 42, 6335-6350, 2008.

7 Bond, T. C., and Bergstrom, R. W.: Light Absorption by Carbonaceous Particles: An Investigative Review, *Aerosol Sci.*

8 *Technol.*, 40, 27-67, 2006.

9 Bond, T. C., Habib, G., and Bergstrom, R. W.: Limitations in the enhancement of visible light absorption due to mixing state,

10 *J. Geophys. Res.-Atmos.*, 111, 2006.

11 Cappa, C. D., Onasch, T. B., Massoli, P., Worsnop, D. R., Bates, T. S., Cross, E. S., Davidovits, P., Hakala, J., Hayden, K. L.,

12 Jobson, B. T., Kolesar, K. R., Lack, D. A., Lerner, B. M., Li, S.-M., Mellon, D., Nuaaman, I., Olfert, J. S., Petäjä, T., Quinn, P.

13 K., Song, C., Subramanian, R., Williams, E. J., and Zaveri, R. A.: Radiative Absorption Enhancements Due to the Mixing State

14 of Atmospheric Black Carbon, *Science,* 337, 1078-1081, 2012.

15 Chen, Y., and Bond, T. C.: Light absorption by organic carbon from wood combustion, *Atmos. Chem. Phys.,* 10, 1773-1787,

16 2010.

17 Cheng, Y. F., Eichler, H., Wiedensohler, A., Heintzenberg, J., Zhang, Y. H., Hu, M., Herrmann, H., Zeng, L. M., Liu, S., Gnauk,

18 T., Brüggemann, E., and He, L. Y.: Mixing state of elemental carbon and non-light-absorbing aerosol components derived from

19 in situ particle optical properties at Xinken in Pearl River Delta of China, *J. Geophys. Res.-Atmos.*, 111, 2006.

20 Cheng, Y. F., Heintzenberg, J., Wehner, B., Wu, Z. J., Su, H., Hu, M., and Mao, J. T.: Traffic restrictions in Beijing during the

21 Sino-African Summit 2006: aerosol size distribution and visibility compared to long-term in situ observations, *Atmos. Chem.*

22 *Phys.,* 8, 7583-7594, 2008.

23 Cheng, Y. F., Su, H., Rose, D., Gunthe, S. S., Berghof, M., Wehner, B., Achtert, P., Nowak, A., Takegawa, N., Kondo, Y.,

24 Shiraiwa, M., Gong, Y. G., Shao, M., Hu, M., Zhu, T., Zhang, Y. H., Carmichael, G. R., Wiedensohler, A., Andreae, M. O., and

25 Pöschl, U.: Size-resolved measurement of the mixing state of soot in the megacity Beijing, China: diurnal cycle, aging and

26 parameterization, *Atmos. Chem. Phys.,* 12, 4477-4491, 2012.

27 Chylek, P., and Wong, J.: Effect of absorbing aerosols on global radiation budget, *Geophys. Res. Lett.*, 22, 929-931, 1995.

28 Drinovec, L., Močnik, G., Zotter, P., Prévôt, A., Ruckstuhl, C., Coz, E., Rupakheti, M., Sciare, J., Müller, T., and Wiedensohler,

29 A.: The" dual-spot" Aethalometer: an improved measurement of aerosol black carbon with real-time loading compensation,

30 *Atmos. Meas. Tech.,* 8, 1965-1979, 2015.

Fuller, K. A., Malm, W. C., and Kreidenweis, S. M.: Effects of mixing on extinction by carbonaceous particles, *J. Geophys. Res.-Atmos.*, 104, 15941-15594, 1999.

Gao, R. S., Schwarz, J. P., Kelly, K. K., Fahey, D. W., Watts, L. A., Thompson, T. L., Spackman, J. R., Slowik, J. G., Cross, E. S., Han, J. H., Davidovits, P., Onasch, T. B., and Worsnop, D. R.: A Novel Method for Estimating Light-Scattering Properties of Soot Aerosols Using a Modified Single-Particle Soot Photometer, *Aerosol Sci. Technol.*, 41, 125-135, 2007.

Gong, X., Zhang, C., Chen, H., Nizkorodov, S. A., Chen, J., and Yang, X.: Size distribution and mixing state of black carbon particles during a heavy air pollution episode in Shanghai, *Atmos. Chem. Phys.,* 16, 5399-5411, 2016.

Gustafsson, Ö., and Ramanathan, V.: Convergence on climate warming by black carbon aerosols, *Proc. Natl. Acad. Sci.* USA, 113, 4243-4245, 2016.

Guo, S., Hu, M., Zamora, M. L., Peng, J., Shang, D., Zheng, J., Du, Z., Wu, Z., Shao, M., Zeng, L., Molina, M. J., and Zhang, R.: Elucidating severe urban haze formation in China, *Proc. Natl. Acad. Sci.* USA, 111, 17373-17378, 2014.

Gysel, M., Laborde, M., Olfert, J. S., Subramanian, R., and Gröhn, A. J.: Effective density of Aquadag and fullerene soot black carbon reference materials used for SP2 calibration, *Atmos. Meas. Tech.*, 4, 2851-2858, 2011.

Huang, X.-F., Xue, L., Tian, X.-D., Shao, W.-W., Sun, T.-L., Gong, Z.-H., Ju, W.-W., Jiang, B., Hu, M., and He, L.-Y.: Highly time-resolved carbonaceous aerosol characterization in Yangtze River Delta of China: Composition, mixing state and secondary formation, *Atmos. Environ.*, 64, 200-207, 2013.

Jacobson, M. Z.: A physically-based treatment of elemental carbon optics: Implications for global direct forcing of aerosols, *Geophys. Res. Lett.*, 27, 217-220, 2000.

Jacobson, M. Z.: Strong radiative heating due to the mixing state of black carbon in atmospheric aerosols, *Nature*, 409, 695-697, 2001.

Jeong, C.-H., Herod, D., Dabek-Zlotorzynska, E., Ding, L., McGuire, M. L., and Evans, G.: Identification of the Sources and Geographic Origins of Black Carbon using Factor Analysis at Paired Rural and Urban sites, *Environ. Sci. Technol.*, 47, 8462-8470, 2013.

Knox, A., Evans, G. J., Brook, J. R., Yao, X., Jeong, C. H., Godri, K. J., Sabaliauskas, K., and Slowik, J. G.: Mass Absorption Cross-Section of Ambient Black Carbon Aerosol in Relation to Chemical Age, *Aerosol Sci. Technol.*, 2009.

Laborde, M., Mertes, P., Zieger, P., Dommen, J., Baltensperger, U., and Gysel, M.: Sensitivity of the Single Particle Soot Photometer to different black carbon types, *Atmos. Meas. Tech.*, 5, 2012.

Lack, D. A., and Cappa, C. D.: Impact of brown and clear carbon on light absorption enhancement, single scatter albedo and absorption wavelength dependence of black carbon, *Atmos. Chem. Phys.*, 10, 4207-4220, 2010.

Lesins, G., Chylek, P., and Lohmann, U.: A study of internal and external mixing scenarios and its effect on aerosol optical properties and direct radiative forcing, *J. Geophys. Res.-Atmos.*, 107, 5-12, 2002.

Li, H., Zhang, Q., Zhang, Q., Chen, C., Wang, L., Wei, Z., Zhou, S., Parworth, C., Zheng, B., Canonaco, F., Prévôt, A. S. H., Chen, P., Zhang, H., Wallington, T. J., and He, K.: Wintertime aerosol chemistry and haze evolution in an extremely polluted

city of the North China Plain: significant contribution from coal and biomass combustion, *Atmos. Chem. Phys.,* 17, 4751-4768, 2017.

Li, M., Zhang, Q., Kurokawa, J. I., Woo, J. H., He, K., Lu, Z., Ohara, T., Song, Y., Streets, D. G., Carmichael, G. R., Cheng, Y., Hong, C., Huo, H., Jiang, X., Kang, S., Liu, F., Su, H., and Zheng, B.: MIX: a mosaic Asian anthropogenic emission inventory under the international collaboration framework of the MICS-Asia and HTAP, *Atmos. Chem. Phys.*, 17, 935-963, 2017.

Liu, D., Allan, J., Whitehead, J., Young, D., Flynn, M., Coe, H., McFiggans, G., Fleming, Z. L., and Bandy, B.: Ambient black carbon particle hygroscopic properties controlled by mixing state and composition, *Atmos. Chem. Phys.,* 13, 2015-2029, 2013.

Liu, D., Whitehead, J., Alfarra, M. R., Reyes-Villegas, E., Spracklen, D. V., Reddington, C. L., Kong, S., Williams, P. I., Ting, Y.-C., Haslett, S., Taylor, J. W., Flynn, M. J., Morgan, W. T., McFiggans, G., Coe, H., and Allan, J. D.: Black-carbon absorption enhancement in the atmosphere determined by particle mixing state, *Nature Geosci.*, 10, 184-188, 2017.

Liu, S., Aiken, A. C., Gorkowski, K., Dubey, M. K., Cappa, C. D., Williams, L. R., Herndon, S. C., Massoli, P., Fortner, E. C., Chhabra, P. S., Brooks, W. A., Onasch, T. B., Jayne, J. T., Worsnop, D. R., China, S., Sharma, N., Mazzoleni, C., Xu, L., Ng, N. L., Liu, D., Allan, J. D., Lee, J. D., Fleming, Z. L., Mohr, C., Zotter, P., Szidat, S., and Prévôt, A. S. H.: Enhanced light absorption by mixed source black and brown carbon particles in UK winter, *Nat Commun.*, 6, 8435, 2015.

Lu, Z., Streets, D. G., Zhang, Q., and Wang, S.: A novel back-trajectory analysis of the origin of black carbon transported to the Himalayas and Tibetan Plateau during 1996–2010, *Geophys. Res. Lett.*, 39, 2012.

McMeeking, G. R., Morgan, W. T., Flynn, M., Highwood, E. J., Turnbull, K., Haywood, J., and Coe, H.: Black carbon aerosol mixing state, organic aerosols and aerosol optical properties over the United Kingdom, *Atmos. Chem. Phys.,* 11, 9037-9052, 2011.

Menon, S., Hansen, J., Nazarenko, L., and Luo, Y.: Climate Effects of Black Carbon Aerosols in China and India, *Science*, 297, 2250-2253, 2002.

Metcalf, A. R., Craven, J. S., Ensberg, J. J., Brioude, J., Angevine, W., Sorooshian, A., Duong, H. T., Jonsson, H. H., Flagan, R. C., and Seinfeld, J. H.: Black carbon aerosol over the Los Angeles Basin during CalNex, *J. Geophys. Res.-Atmos.,* 117, 10.1029/2011JD017255, 2012.

Metcalf, A. R., Loza, C. L., Coggon, M. M., Craven, J. S., Jonsson, H. H., Flagan, R. C., and Seinfeld, J. H.: Secondary Organic Aerosol Coating Formation and Evaporation: Chamber Studies Using Black Carbon Seed Aerosol and the Single-Particle Soot Photometer, *Aerosol Sci. Technol.*, 47, 326-347, 2013.

Moffet, R. C., and Prather, K. A.: In-situ measurements of the mixing state and optical properties of soot with implications for radiative forcing estimates, *Proc. Natl. Acad. Sci.* USA, 106, 11872-11877, 2009.

Moteki, N., and Kondo, Y.: Dependence of Laser-Induced Incandescence on Physical Properties of Black Carbon Aerosols: Measurements and Theoretical Interpretation, *Aerosol Sci. Technol.*, 44, 663-675, 2010.

Moteki, N., Kondo, Y., Miyazaki, Y., Takegawa, N., Komazaki, Y., Kurata, G., Shirai, T., Blake, D. R., Miyakawa, T., and Koike, M.: Evolution of mixing state of black carbon particles: Aircraft measurements over the western Pacific in March 2004, *Geophys. Res. Lett.*, 34, 2007.

Park, S. H., Gong, S. L., Bouchet, V. S., Gong, W., Makar, P. A., Moran, M. D., Stroud, C. A., and Zhang, J.: Effects of black carbon aging on air quality predictions and direct radiative forcing estimation, *Tellus B*, 63, 1026-1039, 2011.

Peng, J., Hu, M., Guo, S., Du, Z., Zheng, J., Shang, D., Levy Zamora, M., Zeng, L., Shao, M., Wu, Y.-S., Zheng, J., Wang, Y., Glen, C. R., Collins, D. R., Molina, M. J., and Zhang, R.: Markedly enhanced absorption and direct radiative forcing of black carbon under polluted urban environments, *Proc. Natl. Acad. Sci.* USA,113, 4266-4271, 2016.

Ram, K., and Sarin, M. M.: Absorption Coefficient and Site-Specific Mass Absorption Efficiency of Elemental Carbon in Aerosols over Urban, Rural, and High-Altitude Sites in India, *Environ. Sci. Technol.*, 43, 8233-8239, 2009.

Ramanathan, V., and Carmichael, G.: Global and regional climate changes due to black carbon, *Nature Geosci.*, 1, 221-227, 2008.

Saliba, G., Subramanian, R., Saleh, R., Ahern, A. T., Lipsky, E. M., Tasoglou, A., Sullivan, R. C., Bhandari, J., Mazzoleni, C., and Robinson, A. L.: Optical properties of black carbon in cookstove emissions coated with secondary organic aerosols: Measurements and modeling, *Aerosol Sci. Technol.*, 50, 1264-1276, 2016.

Sandradewi, J., Prévôt, A. S., Szidat, S., Perron, N., Alfarra, M. R., Lanz, V. A., Weingartner, E., and Baltensperger, U.: Using aerosol light absorption measurements for the quantitative determination of wood burning and traffic emission contributions to particulate matter, *Environ. Sci. Technol.*, 42, 3316-3323, 2008.

Schnaiter, M., Linke, C., Möhler, O., Naumann, K. H., Saathoff, H., Wagner, R., Schurath, U., and Wehner, B.: Absorption amplification of black carbon internally mixed with secondary organic aerosol, *J. Geophys. Res.-Atmos.*, 110, 2005.

Schwarz, J. P., Gao, R. S., Fahey, D. W., Thomson, D. S., Watts, L. A., Wilson, J. C., Reeves, J. M., Darbeheshti, M., Baumgardner, D. G., Kok, G. L., Chung, S. H., Schulz, M., Hendricks, J., Lauer, A., Kärcher, B., Slowik, J. G., Rosenlof, K. H., Thompson, T. L., Langford, A. O., Loewenstein, M., and Aikin, K. C.: Single-particle measurements of midlatitude black carbon and light-scattering aerosols from the boundary layer to the lower stratosphere, *J. Geophys. Res.-Atmos.*, 111, 2006.

Sedlacek, A. J., Lewis, E. R., Kleinman, L., Xu, J., and Zhang, Q.: Determination of and evidence for non-core-shell structure of particles containing black carbon using the Single-Particle Soot Photometer (SP2), *Geophys. Res. Lett.*, 39, 2012.

Segura, S., Estellés, V., Titos, G., Lyamani, H., Utrillas, M. P., Zotter, P., Prévôt, A. S. H., Moˇcnik, G., Alados-Arboledas, L., and Martínez-Lozano, J. A.: Determination and analysis of in situ spectral aerosol optical properties by a multi-instrumental approach, *Atmos. Meas. Tech.*, 7, 2373–2387, 2014.

Seinfeld, J. H., and Pandis, S. N.: Atmospheric Chemistry and Physics: From Air Pollution to Climate Change, 2nd ed. *John Wiley & Sons, Inc.*, New York, 2006.

Shiraiwa, M., Kondo, Y., Iwamoto, T., and Kita, K.: Amplification of Light Absorption of Black Carbon by Organic Coating, *Aerosol Sci. Technol.*, 44, 46-54, 2010.

Shiraiwa, M., Kondo, Y., Moteki, N., Takegawa, N., Miyazaki, Y., and Blake, D. R.: Evolution of mixing state of black carbon in polluted air from Tokyo, *Geophys. Res. Lett.*, 34, 2007.

Sun, Y., Jiang, Q., Wang, Z., Fu, P., Li, J., Yang, T., and Yin, Y.: Investigation of the sources and evolution processes of severe haze pollution in Beijing in January 2013, *J. Geophys. Res.-Atmos.*, 119, 4380-4398, 2014.

Taylor, J. W., Allan, J. D., Liu, D., Flynn, M., Weber, R., Zhang, X., Lefer, B. L., Grossberg, N., Flynn, J., and Coe, H.: Assessment of the sensitivity of core / shell parameters derived using the single-particle soot photometer to density and refractive index, *Atmos. Meas. Tech.*, 8, 1701-1718, 2015.

Wang, L. T., Wei, Z., Yang, J., Zhang, Y., Zhang, F. F., Su, J., Meng, C. C., and Zhang, Q.: The 2013 severe haze over southern Hebei, China: model evaluation, source apportionment, and policy implications, *Atmos. Chem. Phys.,* 14, 3151-3173, 2014a.

Wang, Q., Huang, R. J., Cao, J., Han, Y., Wang, G., Li, G., Wang, Y., Dai, W., Zhang, R., and Zhou, Y.: Mixing State of Black Carbon Aerosol in a Heavily Polluted Urban Area of China: Implications for Light Absorption Enhancement, *Aerosol Sci. Technol.*, 48, 689-697, 2014b.

Weingartner, E., Saathoff, H., Schnaiter, M., Streit, N., Bitnar, B., and Baltensperger, U.: Absorption of light by soot particles: determination of the absorption coefficient by means of aethalometers, *J. Aerosol Sci.*, 34, 1445–1463, 2003

Yang, Y. R., Liu, X. G., Qu, Y., An, J. L., Jiang, R., Zhang, Y. H., Sun, Y. L., Wu, Z. J., Zhang, F., Xu, W. Q., and Ma, Q. X.: Characteristics and formation mechanism of continuous hazes in China: a case study during the autumn of 2014 in the North China Plain, *Atmos. Chem. Phys.*, 15, 8165-8178, 2015.

Yang, Y., Wang, H., Smith, S. J., Ma, P.-L., and Rasch, P. J.: Source attribution of black carbon and its direct radiative forcing in China, *Atmos. Chem. Phys.*, 17, 4319-4336, 2017.

Zhang, G., Bi, X., He, J., Chen, D., Chan, L. Y., Xie, G., Wang, X., Sheng, G., Fu, J., and Zhou, Z.: Variation of secondary coatings associated with elemental carbon by single particle analysis, *Atmos. Environ.*, 92, 162-170, 2014.

Zhang, Q., Streets, D. G., Carmichael, G. R., He, K. B., Huo, H., Kannari, A., Klimont, Z., Park, I. S., Reddy, S., Fu, J. S., Chen, D., Duan, L., Lei, Y., Wang, L. T., and Yao, Z. L.: Asian emissions in 2006 for the NASA INTEX-B mission, *Atmos. Chem. Phys.*, 9, 5131-5153, 2009.

Zhang, R., Khalizov, A. F., Pagels, J., Zhang, D., Xue, H., and McMurry, P. H.: Variability in morphology, hygroscopicity, and optical properties of soot aerosols during atmospheric processing, *Proc. Natl. Acad. Sci.* USA, 105, 10291-10296, 2008.

Zhang, Y., Li, X., Li, M., Zheng, Y., Geng, G., Hong, C., Li, H., Tong, D., Zhang, X., Cheng, Y., Su, H., He, K., and Zhang, Q.: Reduction in black carbon light absorption due to multi-pollutant emission control during APEC China 2014, *Atmos. Chem. Phys. Discuss.*, https://doi.org/10.5194/acp-2018-274, in review, 2018.

Zhang, Y., Zhang, Q., Cheng, Y., Su, H., Kecorius, S., Wang, Z., Wu, Z., Hu, M., Zhu, T., Wiedensohler, A., and He, K.: Measuring the morphology and density of internally mixed black carbon with SP2 and VTDMA: new insight into the absorption enhancement of black carbon in the atmosphere, *Atmos. Meas. Tech.*, 9, 1833-1843, 2016.

1    Zhao, Q., Shen, G., Li, L., Chen, F., Qiao, Y., Li, C., Liu, Q., and Han, J.: Ambient Particles (PM10, PM2.5 and PM1.0) and

2    PM2.5 Chemical Components in Western Yangtze River Delta (YRD): An Overview of Data from 1-year Online Continuous

3    Monitoring at Nanjing, *Aerosol Sci. Eng.,* 2017.

4    Zhao, X. J., Zhao, P. S., Xu, J., Meng, W., Pu, W. W., Dong, F., He, D., and Shi, Q. F.: Analysis of a winter regional haze event

5    and its formation mechanism in the North China Plain, *Atmos. Chem. Phys.,* 13, 5685-5696, 2013.

6    Zheng, G., Duan, F., Ma, Y., Zhang, Q., Huang, T., Kimoto, T., Cheng, Y., Su, H., and He, K.: Episode-Based Evolution Pattern

7    Analysis of Haze Pollution: Method Development and Results from Beijing, China, *Environ. Sci. Technol.*, 50, 4632-4641,

8    2016.

9    Zheng, G. J., Duan, F. K., Su, H., Ma, Y. L., Cheng, Y., Zheng, B., Zhang, Q., Huang, T., Kimoto, T., Chang, D., Pöschl, U.,

10    Cheng, Y. F., and He, K. B.: Exploring the severe winter haze in Beijing: the impact of synoptic weather, regional transport

11    and heterogeneous reactions, *Atmos. Chem. Phys.*, 15, 2969-2983, 2015.

1 **Table 1.** The average PM$_1$ mass concentration, rBC mass concentration, normalized $EEI_{total}$, $EEI_{adjacent}/EEI_{total}$ ratio, the mass-

2 averaged values of the $D_p/D_c$ ratio and calculated $E_{ab}$ during clean, slightly polluted and polluted periods. $EEI_{adjacent}$ is the EEI

3 of BC from areas outside Beijing; the $EEI_{ouside}/EEI_{total}$ ratio reflects the amount of BC contributed by regional transport to the

4 total amount of BC observed at our site. The clean (PM$_{2.5} \le$ 35 μg m$^{-3}$), slightly polluted (35 μg m$^{-3}$ < PM$_{2.5} \le$ 115 μg m$^{-3}$) and

5 polluted (PM$_{2.5}$ > 115 μg m$^{-3}$) periods were classified according to the Air Quality Index (Zheng et al. 2015).

|  | Clean | Slightly polluted | Polluted |
|---|---|---|---|
| PM$_1$ (μg m$^{-3}$) | 12.57 | 54.26 | 141.93 |
| rBC (μg m$^{-3}$) | 0.82 | 2.89 | 6.07 |
| Normalized $EEI_{total}$ | 3.68 | 9.19 | 16.87 |
| $EEI_{outside}/EEI_{total}$ | 0.21 | 0.39 | 0.63 |
| $D_p/D_c$ | 1.62 | 1.81 | 2.04 |
| Calculated $E_{ab}$ | 1.66 | 1.81 | 1.91 |
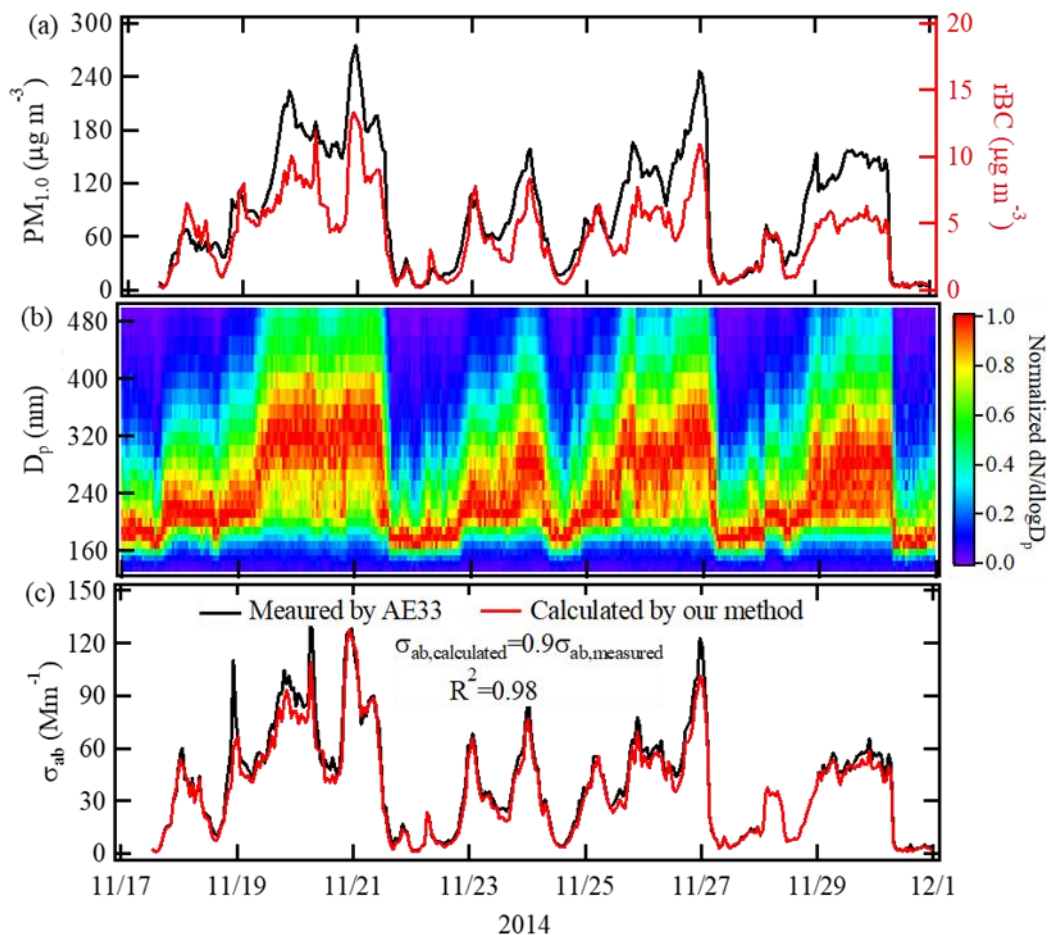
2     **Figure 1.** Time series of (a) the PM$_1$ and rBC mass concentrations, (b) the diameter of BC-containing particles ($D_p$) and (c)

3     the light absorption coefficient ($\sigma_{ab}$) at 880 nm. The correlation between the calculated $\sigma_{ab}$ ($\sigma_{ab, calculated}$) using Mie theory

4     combined with SP2 measurements and the measured $\sigma_{ab}$ ($\sigma_{ab, measured}$) by the AE33 is also shown in (c).
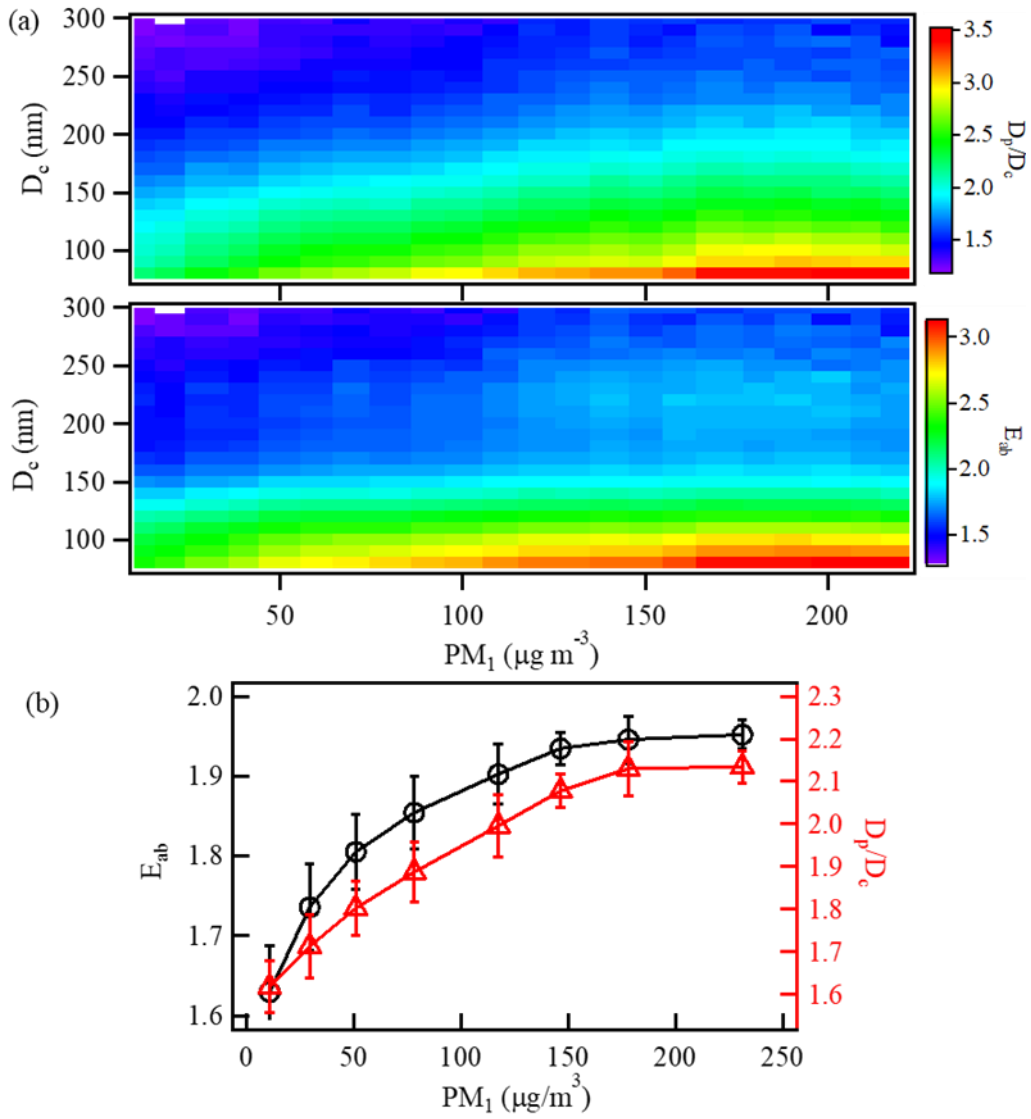
2 **Figure 2.** (a) The aging degree ($D_p/D_c$ ratio) and light absorption enhancement (calculated $E_{ab}$) of BC-containing particles with size-resolved
3 rBC cores ($D_c$) under different PM$_1$ concentration (28 samples); (b) Variations in the mass-averaged values of the $D_p/D_c$ ratio and calculated
4 $E_{ab}$ of BC-containing particles with PM$_1$ concentration.
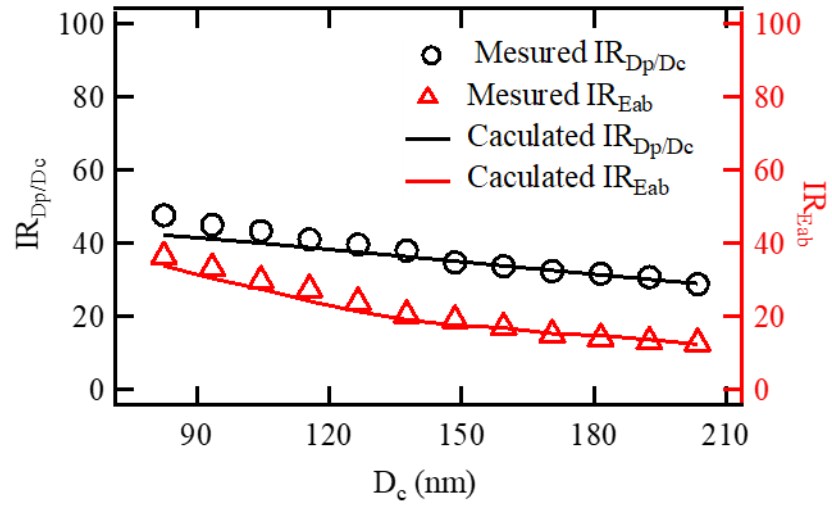
2 **Figure 3.** The increase ratio of the $D_p/D_c$ and and calculated $E_{ab}$ ($IR_{Dp/Dc}$ and $IR_{Eab}$) for BC-containing particles with $PM_1$

3 concentration increasing from 10 μg m$^{-3}$ to 230 μg m$^{-3}$. The calculated $IR_{Dp/Dc}$ and $IR_{Eab}$ was determined based on Eqs. (13)

4 and (14). The measured $IR_{Dp/Dc}$ and $IR_{Eab}$ was obtained from SP2 measurements.
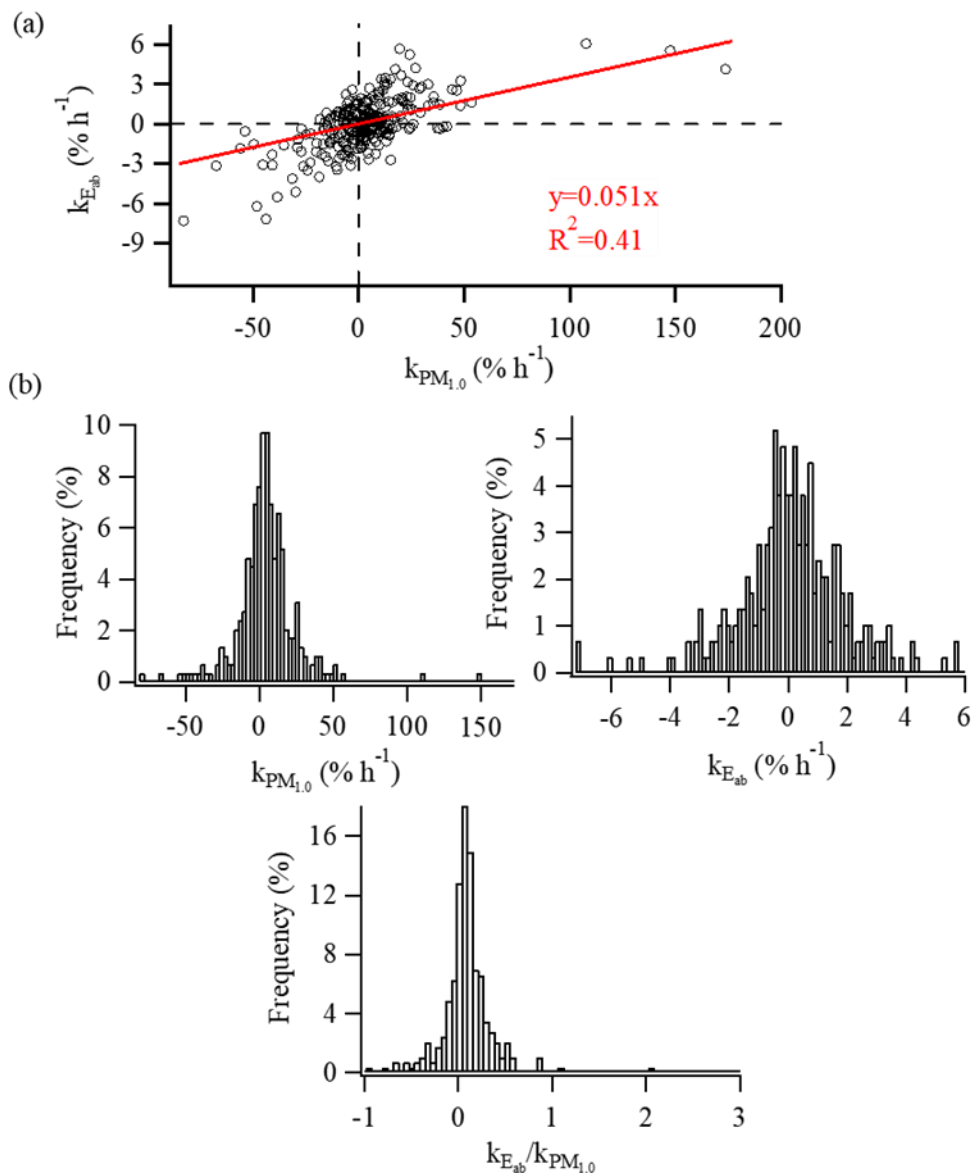
2 Figure 4. (a) Correlation between the changing rate of calculated $E_{ab}$ ($k_{Eab}$) and the changing rates of $PM_1$ concentrations ($k_{PM1}$) during the

3 campaign period. (b) Frequency distribution of $k_{Eab}$, $k_{PM1}$, and $k_{Eab}/k_{PM1}$. The $k_{Eab}$ and $k_{PM1}$ values represent an apparent changing rate of

4 calculated $E_{ab}$, $PM_1$ concentration and rBC mass concentration, respectively, and are from point-by-point differences of hourly $E_{ab}$, namely

5 $k_{Eab} = (E_{ab,t2}-E_{ab,t1})/(E_{ab,t1}*(t_2-t_1))$ and $k_{PM1} = (PM_{1,t2}- PM_{1,t1})/(PM_{1,t1}*(t_2-t_1))$. The sensitivity of the change of calculated $E_{ab}$ with changing

6 $PM_1$ concentrations was obtained by plotting $k_{Eab}$ vs. $k_{PM1}$ (i.e., $k_{Eab}/k_{PM1}$, the slope shown in (a)).
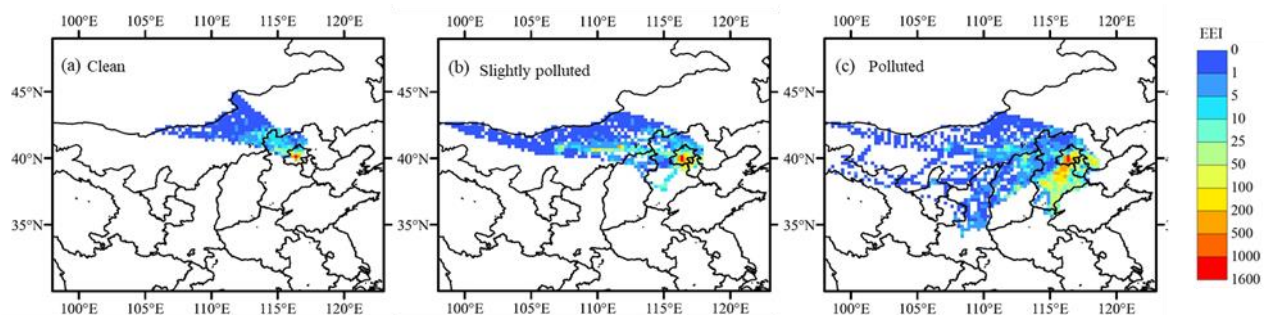
2    Figure 5. Spatial distribution (0.25°×0.25°) of the effective emission intensity (EEI, unit of ton/grid/year) for BC transported

3    to the observation site (40º00'17" N, 116º19'34" E) during clean, slightly polluted and polluted periods. The clean (PM$_{2.5}$ ≤

4    35 µg m$^{-3}$), slightly polluted (35 µg m$^{-3}$ < PM$_{2.5}$ ≤ 115 µg m$^{-3}$) and polluted (PM$_{2.5}$ > 115 µg m$^{-3}$) periods were classified

5    according to the Air Quality Index (Zheng et al. 2015). The site location and the boundaries of the in-region (i.e., Beijing) vs.

6    outside of region (i.e., other areas such as Tianjin, Heibei, Inner Mongolia, Shanxi, Shandong), shown in Fig. S1. Noted that

7    these regions are defined based on political boundaries.
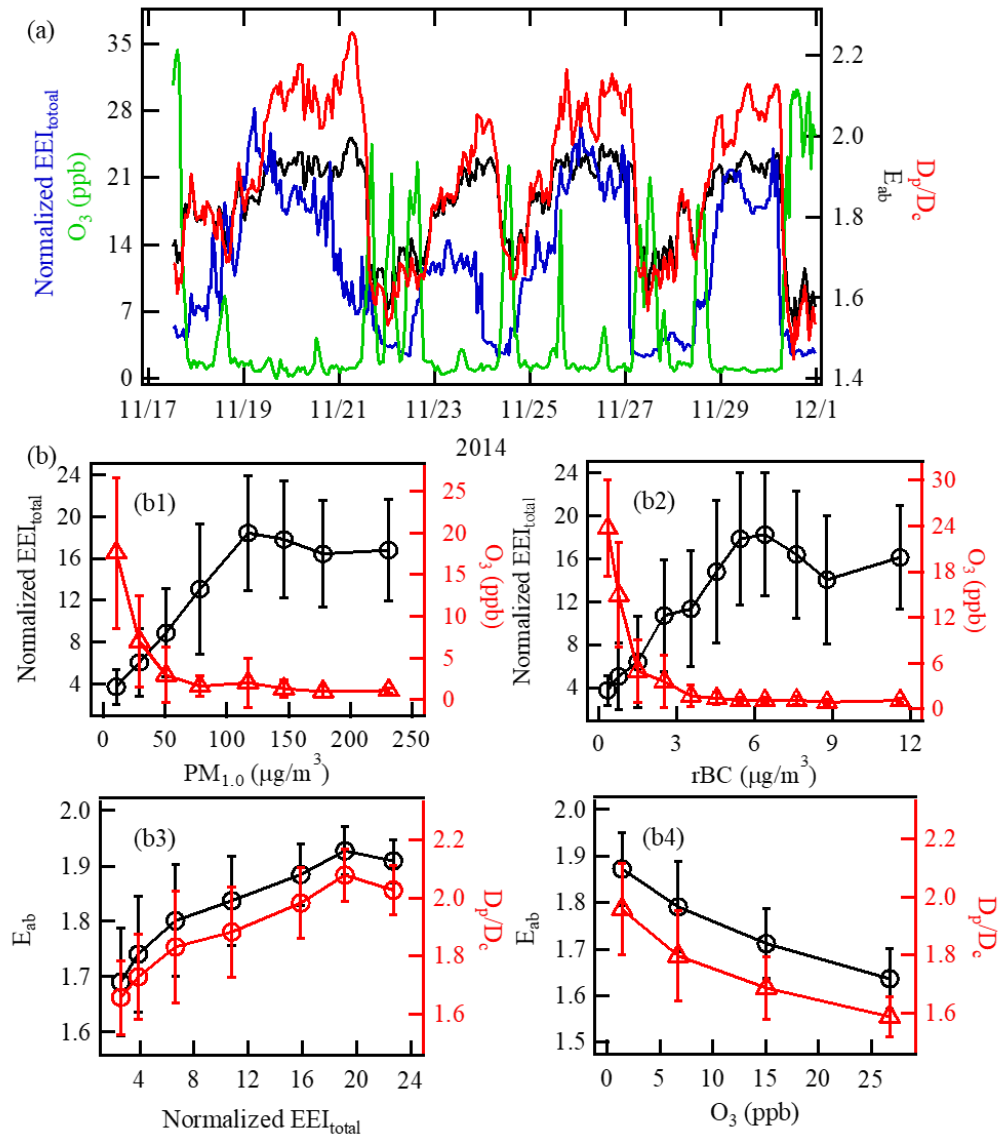
Figure 56. (a) Time series of the normalized $EEI_{total}$, $D_p/D_c$ rations and $E_{ab}$ of BC-containing particles and the $O_3$ concentration

during the campaign period. (b) Variations in the $D_p/D_c$ and $E_{ab}$ of BC-containing particles with the normalized $EEI_{total}$ and $O_3$

concentration. Normalized $EEI_{total}$ ($EEI_{total,normalized}$) was calculated by scaling by a factor of $10^{-3}$, namely $EEI_{total,normalized} =$

$EEI_{total}/1000$.
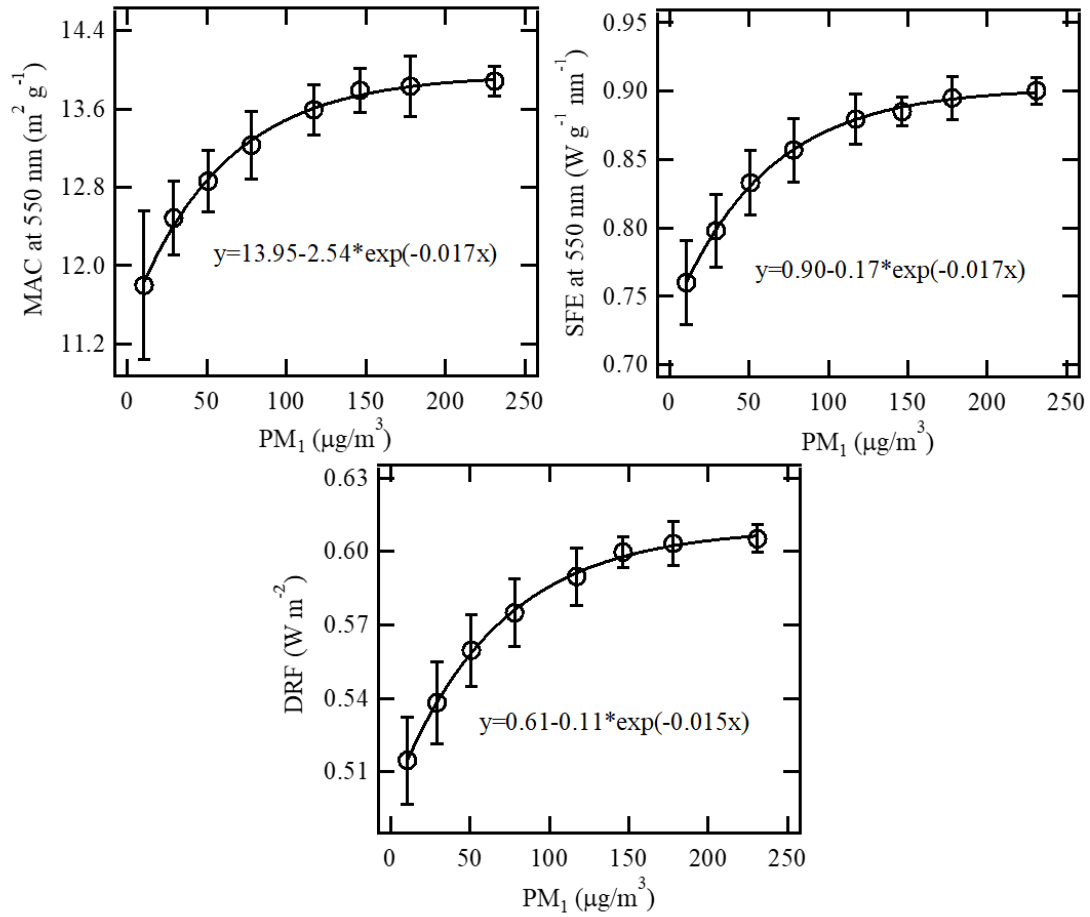
**Figure 7.** Variations in the *MAC*, *SFE* and *DRF* of BC-containing particles with the $PM_1$ concentrations. The DRF values for BC-containing particles at different pollution levels were obtained by scaling the average *DRF* (0.31 W m$^{-2}$, Table S1) of externally mixed BC from various climate models (Bond et al., 2013) with a scaling factor of $E_{ab}$ under different $PM_1$ concentrations. In order to point out the effect of BC light-absorption capability on DRF under different PM1 concentrations, we did not consider the changes of total BC amount for DRF calculation in (c).

3   **Figure 8.** Conceptual scheme of amplification effect on BC light absorption associated with air pollution.